Kinetics of Antigen Expression and Epitope Presentation during Virus Infection

Nathan P. Croft[1], Stewart A. Smith[2], Yik Chun Wong[2], Chor Teck Tan[1], Nadine L. Dudek[1], Inge E. A. Flesch[2], Leon C. W. Lin[2], David C. Tscharke[2¶]*, Anthony W. Purcell[1¶]*

1 Department of Biochemistry and Molecular Biology, Monash University, Clayton, Victoria, Australia, 2 Research School of Biology, The Australian National University, Canberra, Australian Capital Territory, Australia

Abstract

Current knowledge about the dynamics of antigen presentation to T cells during viral infection is very poor despite being of fundamental importance to our understanding of anti-viral immunity. Here we use an advanced mass spectrometry method to simultaneously quantify the presentation of eight vaccinia virus peptide-MHC complexes (epitopes) on infected cells and the amounts of their source antigens at multiple times after infection. The results show a startling 1000-fold range in abundance as well as strikingly different kinetics across the epitopes monitored. The tight correlation between onset of protein expression and epitope display for most antigens provides the strongest support to date that antigen presentation is largely linked to translation and not later degradation of antigens. Finally, we show a complete disconnect between the epitope abundance and immunodominance hierarchy of these eight epitopes. This study highlights the complexity of viral antigen presentation by the host and demonstrates the weakness of simple models that assume total protein levels are directly linked to epitope presentation and immunogenicity.

Introduction

The presentation of virus peptides (epitopes) to CD8^{+} T cells plays a pivotal role in anti-viral immunity. Recognition of these epitopes presented on MHC class I drives CD8^{+} T cell priming following interactions with professional antigen presenting cells (APC) and subsequently allows control of infection through killing of infected cells and secretion of cytokines. The process of MHC class I antigen presentation is complex and multi-staged. It starts with degradation of polypeptides, typically by the proteasome, followed by transport to the ER, loading onto MHC class I and finally egress to the cell surface [1]. Along the way other proteases and chaperones refine the peptides and perform quality control functions on peptide-MHC complexes (pMHC) [2]. Surprisingly, despite the large coding capacity and therefore antigenic potential of many viruses, CD8^{+} T cell responses are often skewed towards a small number of peptides in a phenomenon known as immuno-dominance [3]. This is exemplified by studies of humans and animals infected with large, complex dsDNA viruses, such as herpes- and poxviruses, where reproducible CD8^{+} immunodomi-nance hierarchies emerge. For example, up to 20% of the CD8^{+} T cell response following infection of C57BL/6 mice with vaccinia virus (VACV) is directed towards a single immunodominant epitope and a handful of subdominant specificities account for much of the remainder [4,5]. Further, while MHC class I antigen

presentation is well understood in principle [6] and bioinformatic predictions of MHC class I binding are often highly refined [7], prediction of antigenicity and immunogenicity have remained elusive.

In part this gap remains because kinetic studies to date have focused on single peptides [8] and broader scale studies of antigenicity have been limited to single time points [9–11]. This has reflected limitations of technology in that the best reagents for quantifying antigen presentation have been the few monoclonal antibodies generated to date that recognise specific pMHC complexes [8,12–15]. Proteome-wide biochemical approaches have typically required prohibitively large numbers of cells (1×10^9 and greater) restricting experiments to single time points [16,17] . Although we have good examples showing the diversity of native virus epitopes presented and we know the consequences of manipulating expression levels and even translation rates for presentation of model antigens [8,18], this information remains disconnected. As a consequence, while it is clear that increasing expression of a given antigen leads to higher presentation of epitopes, it is not known whether antigen expression level *per se* is a useful predictor of likely antigenicity across different viral proteins. Further, whether bulk protein abundance or expression levels correlate best with production of epitopes as a general rule is not known. Indeed, several recent studies have highlighted the diversity of source for MHC class I bound peptides and have

Author Summary

A major mechanism for the detection of virus infection is the recognition by T cells of short peptide fragments (epitopes) derived from the degradation of intracellular proteins presented at the cell surface in a complex with class I MHC. Whilst the mechanics of antigen degradation and the loading of peptides onto MHC are now well understood, the kinetics of epitope presentation have only been studied for individual model antigens. We addressed this issue by studying vaccinia virus, best known as the smallpox vaccine, using advanced mass spectrometry. Precise and simultaneous quantification of multiple peptide-MHC complexes showed that the surface of infected cells provides a surprisingly dynamic landscape from the point of view of anti-viral T cells. Further, concurrent measurement of virus protein levels demonstrated that in most cases, peak presentation of epitopes occurs at the same time or precedes the time of maximum protein build up. Finally, we found a complete disconnect between the abundance of epitopes on infected cells and the size of the responding T cell populations. These data provide new insights into how virus infected cells are seen by T cells, which is crucial to our understanding of anti-viral immunity and development of vaccines.

implicated both products of translational infidelity (defective ribosome initiation products (DRiPs)) [10,19–22] as well as mature proteins [23]. For instance, some biochemical surveys of epitope versus transcript or steady-state antigen abundance suggest these are closely related at single time points [16,24]. However, most epitopes studied in detail are shown to be the products of recent translation and therefore need not be related to final antigen abundance [25–28]. Only studies that can link the kinetics of antigen synthesis and accumulation with epitope presentation for multiple native virus proteins will allow general conclusions to be drawn. Finally, antigen expression levels can be linked to immunogenicity for model antigens, but again whether this is useful for evaluating whole viral proteomes has not been approached.

Here we present the first study that links the kinetics of virus protein build up and CD8+ T cell epitope presentation for multiple pMHC complexes. We used vaccinia virus, best known as the vaccine used to eradicate smallpox, taking advantage of its robust *in vitro* infections and a well characterised CD8+ T cell epitope hierarchy [4,5]. In addition there is good evidence that anti-VACV CD8+ T cells are directly primed by infected APC making this an ideal choice to study antigen presentation *in vitro* [29–31]. The abundance of 8 VACV epitopes was quantified simultaneously at multiple times after infection using the multiple reaction monitoring approach to tandem mass spectrometry [32]. The same method was applied in parallel to determine relative abundance of the relevant virus proteins using filter assisted sample preparation and whole cell tryptic digestion [33]. Together, these data provide an unparalleled insight into the dynamic nature of antigen presentation on class I during a virus replication cycle. Further they provide the most compelling evidence to date of the direct correlation between the timing of virus antigen expression and the appearance of epitopes derived from the same protein. Finally, while we can now add kinetics to our description of epitope presentation for multiple epitopes, these biochemical data still fail to predict the hierarchy of immunodominance in responding CD8+ T cell responses.

Results

Antigen presentation during viral infection is complex and cannot be described by a single epitope

Previous studies aimed at understanding antigen presentation kinetics have focussed on single epitopes, most commonly the model peptide SIINFEKL (presented by H-2K^b) expressed from recombinant viruses, including VACV. Whilst these experiments have yielded much useful mechanistic insight, it is not clear whether kinetic data generated are representative of virus epitopes in general. To examine this issue, we first recapitulated published data showing the rapid rise of H-2K^b-SIINFEKL complexes on cells infected with a recombinant VACV strain WR-NP-S-GFP [8,13]. This virus expresses a chimera in which SIINFEKL is sandwiched between influenza virus nucleoprotein and enhanced green fluorescent protein [8,34]. DC2.4 cells, a dendritic cell-like line derived from C57BL/6 mice, were infected at a multiplicity of 10 pfu per cell and presentation of K^b-SIINFEKL complexes measured using the mAb 25D1.16 and flow cytometry at various times (Figure 1A). Consistent with previous work that typically used L-K^b cells, in DC2.4 K^b-SIINFEKL complexes rose rapidly after infection and began to plateau by 6 hours post infection (hpi). To test if the kinetics observed for K^b-SIINFEKL complexes is representative of all VACV epitopes we used polyclonal T cells isolated from infected mice since monoclonal antibodies to VACV epitope-MHC complexes are not available. If all VACV antigen presentation is like K^b-SIINFEKL, the fraction of polyclonal anti-VACV CD8+ T cells that can be stimulated by infected cells should rise over time with a simple, rapid kinetic. If on the other hand, new pMHC complexes first appear on the cell surface at different times after infection, then one might expect a more complicated curve as new populations of T cells are able to be activated once their epitope appears at the cell surface. Thus using DC2.4 and the same infection protocol, global VACV epitope presentation was probed up to 12 hpi using splenocytes taken from mice seven days after VACV infection and the percent of CD8+ T cells making IFNγ determined by intracellular cytokine staining (ICS) (Figure 1B). In contrast to the simple rise of K^b-SIINFEKL presentation, the increase in number of CD8+ T cells recognising the infected cells was more complex. There were two phases of rising CD8+ T cell activation, one from 2 to 5 hours (a similar time frame to K^b-SIINFEKL presentation) followed by second, steeper rise from 5–7 hpi that continued until 12 hpi. While this reveals nothing about the kinetics of individual epitopes, it suggests that the onset of presentation differs across the native VACV epitopes. It is also consistent with published work using mono-specific T cell lines that shows presentation of some VACV epitopes is delayed for some hours after infection [35]. Together these data suggest that monitoring a single epitope does not reveal the true complexity of viral antigen presentation to T cells. We therefore sought to dissect in greater detail the presentation of individual VACV derived epitopes using mass spectrometry (MS).

LC-MRM for the simultaneous detection and quantitation of multiple VACV epitopes

Liquid chromatography coupled to multiple reaction monitoring mass spectrometry (LC-MRM) is the method of choice for detection of multiple known peptides [32,36,37]. LC-MRM MS affords high sensitivity and selectivity and has been recently applied to multiplexed qualitative and quantitative analyses of peptide epitopes eluted from MHC molecules [32,37]. For this study, eight VACV epitopes restricted by murine H-2 K^b were chosen based on their well characterised immunogenicity and their expression from a variety of different VACV proteins spanning
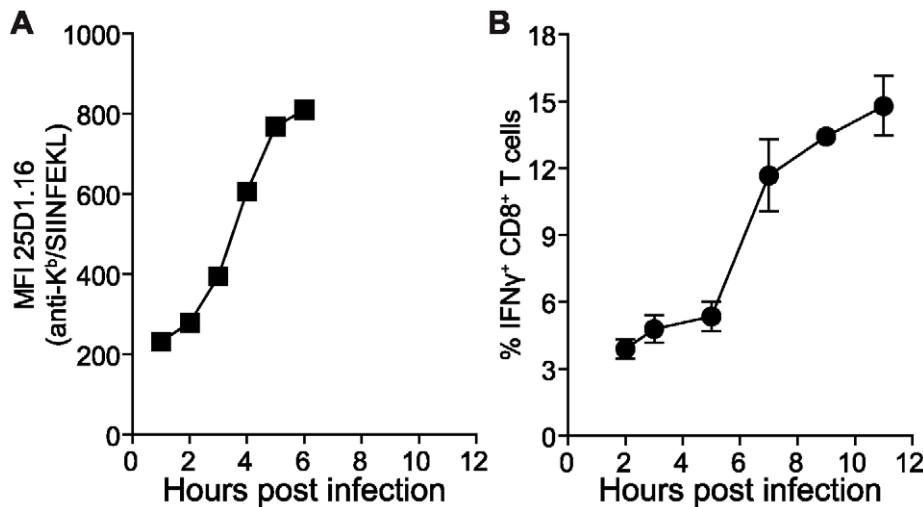
Figure 1. Antigen presentation during virus infection is complex and cannot be described by a single epitope. DC2.4 cells were infected with VACV strain WR-NP-S-GFP (A) or WR (B) and presentation of MHC class I peptides detected at various times. A) K^b-SIINFEKL presentation levels determined by staining with mAb 25-D1.16 and flow cytometry. Data are representative multiple experiments. B) Presentation of bulk native VACV epitopes determined by incubation with VACV-immune splenocytes and detecting activation by staining for surface $CD8^+$ and intracellular IFNγ. Means and SEM of triplicates are shown and the data are representative of two independent experiments.
doi:10.1371/journal.ppat.1003129.g001

different temporal phases of the infection (Table 1) [4,5]. In addition, SIINFEKL was included in some experiments to allow a direct comparison of this model antigen with the native VACV epitopes. Optimal MRM transition conditions (precursor ion charge, fragmentation energy and fragment ion selection) for each VACV epitope listed in Table 1 were determined using synthetic peptides (Table S1 and Figure S1 in Supporting Information). The resulting MRM method allowed for the simultaneous detection of all 8 VACV epitopes (Figure 2A) and also included transitions to measure SIINFEKL and isotopically-labelled (AQUA) SIIN*FEKL; inclusion of the SIIN*FEKL AQUA peptide was used to control for losses during processing of the MHC-bound peptides as described [32]. The unequivocal detection of peptide epitopes was achieved by several rigorous confirmatory steps in this LC-MRM workflow: firstly, RP-HPLC retention across multiple dimensions of purification (correct eluting fraction during off-line RP-HPLC and correct on-line retention time during LC-MRM MS) must be consistent with that measured for the synthetic version of each of the VACV peptides (Figure S2); secondly, they must trigger all MRM transitions concurrently and in the correct transition hierarchy; and, as a final step, each peptide sequence must be further confirmed by an MRM-triggered MS/MS sequencing scan – a modality unique to the quadrupole linear ion trap mass spectrometer used in this study [38].

Validation of LC-MRM and detection of VACV epitopes eluted from cells

In order to verify the sample workflow (Figure 2B), DC2.4 cells were incubated with a pooled mixture of the full set of 8 synthetic peptides representing VACV epitopes (Table 1). Following extensive washing to remove unbound peptides, cells were pelleted and snap-frozen and subjected to immunoaffinity purification of H-2K^b complexes, peptide elution and chromatographic separation as previously described [32,37]. The presence of each VACV epitope in the MHC eluate was confirmed by LC-MRM (Figure 2C). The differing detection intensities across the peptide set reflects a combination of the varying ionisation efficiencies of the peptides and competition for binding to the K^b molecules during incubation.

Next, MHC elution and LC-MRM were used for the detection of SIINFEKL and native VACV epitopes generated through VACV infection with the recombinant WR-NP-S-GFP. DC2.4 cells (1×10^8) were infected for 6 hours with WR-NP-S-GFP to compare the levels of SIINFEKL presentation with that of the 8 native VACV epitopes (Figure 3). Capture of K^b-peptide complexes was achieved as above, including the addition of 50 fmol of isotopically-labelled AQUA SIIN*FEKL in order to control for sample preparation losses post affinity purification of the MHC-peptide complexes [32]. The quantification of each VACV epitope was achieved by comparing the area under the MRM curve to that of 100 fmol of the corresponding synthetic epitope analysed separately (Figure 2A). LC-MRM confirmed the detection of SIINFEKL and all 8 VACV peptides (Figure 3A shows representative data for SIINFEKL, $B8_{20-27}$ and $J3_{289-296}$). Further it provides the first definitive evidence that the amino acid length and constitution of the VACV epitopes is exactly as described in the original mapping studies [4,5]. SIINFEKL presentation on WR-NP-S-GFP-infected cells at 6 hpi was calculated to be 2.3×10^4 and 3.1×10^4 copies per cell for two independent experiments (Figure 3B). All 8 K^b-restricted VACV epitopes were detected at considerably lower estimated abundances to that of SIINFEKL. Further, abundance of the 8 VACV peptides varied over a wide range with 3 epitopes ($B8_{20-27}$; $A47_{138-146}$ and $J3_{289-296}$) being presented at levels up to 1000-fold higher than the remaining 5 VACV epitopes. When compared to $CD8^+$ T cell response elicited in mice infected for 7 days by the same virus, there is a striking dissociation between the epitope abundance and T cell immunodominance hierarchies (Figure 3B).

Kinetics of VACV epitope and protein presentation

Next we sought to assess the presentation kinetics of the 8 VACV epitopes during the course of infection. This was done using non-recombinant VACV, to avoid any potential competing effects from the very high levels of presentation of SIINFEKL following infection with the recombinant WR-NP-S-GFP VACV strain. DC2.4 cells were infected for 0.5, 3.5, 6.5, 9.5 and 12.5 hours, or mock infected as a negative control and epitope

Table 1. VACV CD8^{+} T cell epitopes.

Epitope	Sequence	IC$_{50}$ (nM)	Protein Function	Expression*	Promoter**
B8$_{20-27}$	TSYKFESV	K^b, 1.1	Immune modulator	E1.1	E
A8$_{189-196}$	ITYRFYLI	K^b, 6.2	Viral transcription factor	E1.1	E
A3$_{270-277}$	KSYNYMLL	K^b, 2.7	Virion core protein	PR	I
C4$_{125-132}$	LNRFENV	K^b, 0.84	Unknown	E1.2	E
A47$_{138-146}$	AAFEFINSL	K^b, 0.61	Unknown	E1.2	E
L2$_{53-61}$	VIYIFTVRL	K^b, 0.85	Unknown	E1.1	E
J3$_{289-296}$	SIFRFLNI	K^b, 1.2	Viral RNA pol component	E1.2	E
A19$_{47-55}$	VSLDYINTM	K^b, 0.94	Unknown	PR	I

*[41] Expression time based on cluster analysis of transcript levels during infection. E1.1 and E1.2 are early classes, with E1.1 expressed earlier and at higher levels that E1.2. PR (post replication), typically referred to as the late class.
**[43] Earliest promoter associated with gene. E is early, I is intermediate.
doi:10.1371/journal.ppat.1003129.t001

abundance at each time determined by LC-MRM analysis. All 8 VACV epitopes were detected and the kinetics of their presentation measured (Figure 4A). Six of 8 peptides were detected by 0.5 hpi, with the remaining 2 epitopes (A3$_{270-277}$ and A19$_{47-55}$) undetectable until 6 hours later. Peak expression occurred at 3.5 hpi for 5 epitopes, 6.5 hpi for two epitopes and at the final time point of 12.5 hours for a single epitope. We noted that the presentation of the immunodominant B8$_{20-27}$ epitope was unusual in that its onset was at 30 minutes, but instead of peaking at 3.5 hpi, like most of this group of epitopes, its peak was later at 6.5 hpi. The abundance profile spanned 3 logs, ranging from as

low as an estimated 11 copies per cell for C4$_{125-132}$ to as high as 32,400 copies of A47$_{138}$. These basic features of presentation with some epitopes showing peak presentation around 3.5 hours after infection, while others only appear at 6.5 hours have also been observed for cells infected with the MVA strain of VACV (our unpublished observations). Thus abundance and kinetics of presentation are highly variable across different epitopes and robust presentation early after infection is not always maintained.

In order to assess how the kinetics of epitope presentation correlates with source antigen expression, a sample of the cell lysate from each infection time point was subjected to reduction,
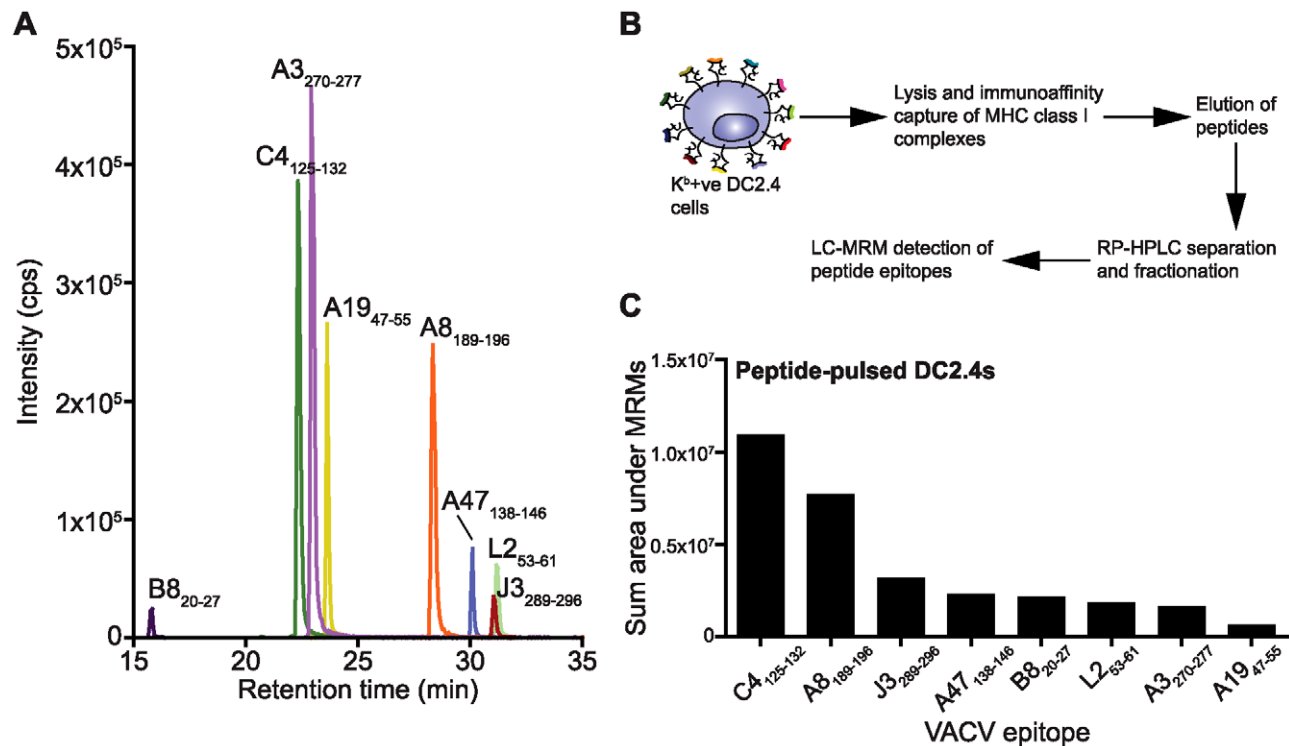
Figure 2. Simultaneous detection of multiple viral epitopes by LC-MRM MS. A) Demonstration of multiplexed detection of 8 VACV K^b-binding epitopes. A mixture of 100 fmol of each synthetic peptide was loaded and analysed directly by LC-MRM using a method to detect all peptides simultaneously. A single MRM transition per peptide is shown for clarity. B) Schematic of sample workflow. C) DC2.4 cells were pulsed with a 1 µM mixture of each VACV peptide, incubated for 1 hour and washed extensively to remove unbound peptide. Cells were subjected to MHC-peptide elution and each epitope detected by LC-MRM-MS (sum area of all MRM transitions per peptide is shown).
doi:10.1371/journal.ppat.1003129.g002
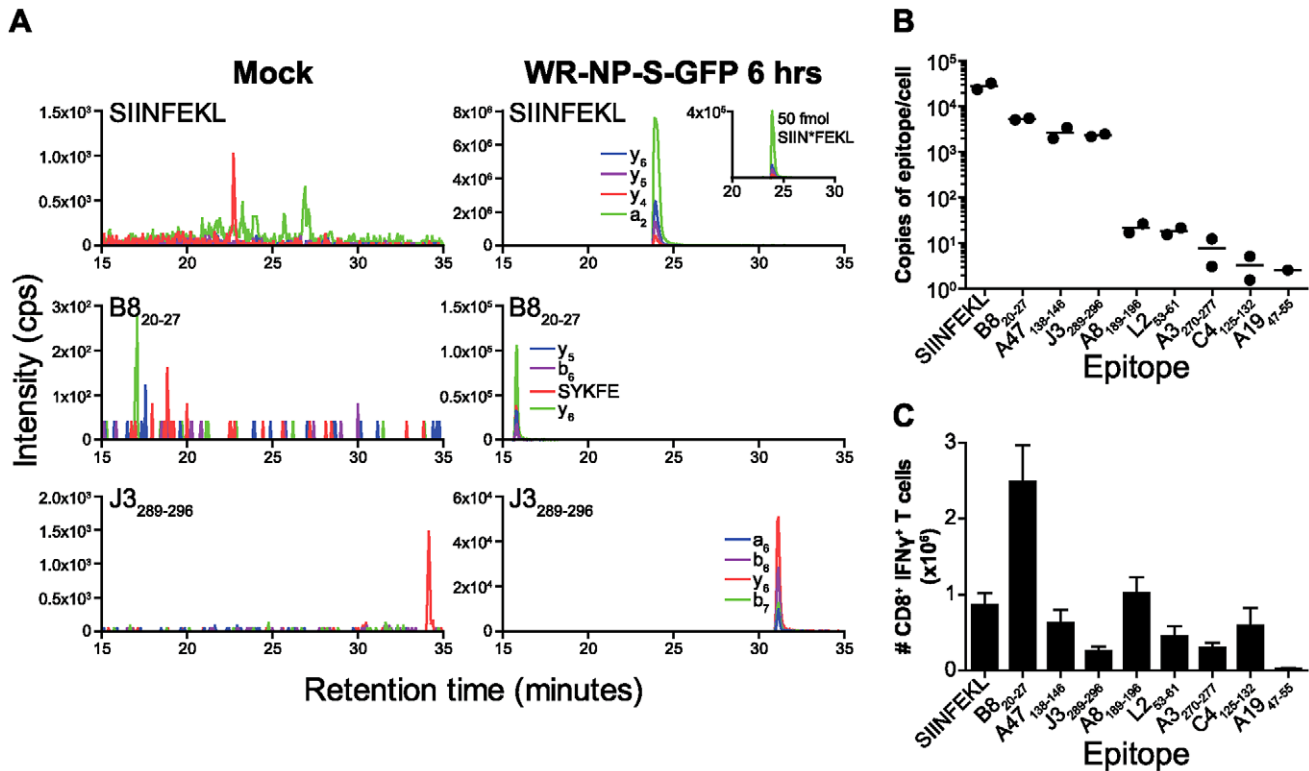
Figure 3. Detection and quantitation of SIINFEKL and VACV epitopes from WR-NP-S-GFP infection. 1×10^8 DC2.4 cells were either mock treated or infected with 5 pfu of VACV strain WR-NP-S-GFP for 6 hours and epitopes eluted and analysed by the LC-MRM workflow. A) Representative MRM traces for the detection of SIINFEKL (RP-HPLC fraction A10) and VACV epitopes B8$_{20-27}$ (fraction A8) and J3$_{289-296}$ (fraction A13). Background, non-specific MRM signal is shown for mock treatment (left panels). Positive, overlapping MRM transitions (four per peptide, Q3 ions as indicated) are shown during infection (right panels). Inset: MRM signal for 50 fmol of the internal standard isotopically-labelled AQUA peptide SIIN*FEKL for the absolute quantitation of SIINFEKL levels. B) Epitope presentation hierarchy on DC2.4 cells 6 hours after infection with WR-NP-S-GFP by LC-MRM. Data from 2 independent infections are shown. C) CD8$^+$ T cell immunodominance hierarchy 7 days after infection of C57BL/6 mice as determined by brief stimulation with the peptides shown and ICS for IFNγ. Data are the mean and SEM of 3 mice and are representative of two experiments. doi:10.1371/journal.ppat.1003129.g003

alkylation and subsequent digestion with the enzyme trypsin prior to proteomic analysis. Proteotypic tryptic fragments from each of the 8 VACV protein antigens were chosen using Skyline [39] (Table S2 and Figures S3 and S4). Following initial screening of samples, 6 of the 8 VACV proteins were detected (for A3 and J3, multiple tryptic fragments were found to be amenable to MRM analysis and so all were included). Despite rigorous testing of multiple peptides, no positive signal could be detected for proteins L2 and C4 so these were not included further. In order to achieve normalisation of protein loading across the timecourse, 12 murine tryptic peptides (corresponding to eight host proteins; Table S3 and Figure S3) were simultaneously analysed in the same LC-MRM method (Figure S3). These murine proteins were chosen as suitable candidates for normalisation based on the high copy number and long half life of their human homologues [40], with the notion that such proteins will not be grossly affected by the VACV-mediated shutdown of host protein synthesis. In addition, a good correlation between the abundance of these representative proteins and cell number recovered post-infection was found suggesting that they were appropriate for normalisation (Figure 3C). The uncorrected data is also shown in Figure S4 for comparison.

MRM peaks at each time point for the 6 VACV proteins were used to determine relative protein expression over the course of infection and these were plotted alongside the relative levels of each epitope derived from the same protein (Figure 4B). This approach allows relative expression of individual antigens to be determined at different time points but does not provide absolute quantitation of the antigen and therefore direct comparison between antigens is more qualitative. Expression profiles of the 6 proteins were consistent with their temporal expression cluster as reported by analyses of transcription and more recently defined promoters [41–43], which gives further confidence of the method. Translation, as determined by tryptic peptide detection, was detected at 0.5 hpi for A47, A8 and B8, corresponding with the appearance of epitopes derived from those proteins. Whilst levels of A47 peaked at 6.5 hpi, all other proteins peaked (at least within the limits of this time course) at 12.5 hours. Proteins A3 and A19, both of which are classified as late, were detected by 3.5 hours, but did not reach substantial levels until 6.5 hours and onwards; presentation of epitopes A3$_{270-277}$ and A19$_{47-55}$ tracked closely with the increase in protein levels. For epitopes A47$_{138-145}$, A8$_{189-196}$ and J3$_{125-132}$, rapid and peak presentation following protein expression was followed by a sharp decline in epitope levels to almost zero by 12.5 hpi. However, epitopes B8$_{20-27}$ and A3$_{270-277}$, although decreasing following peak levels mid-infection, maintained a more constant level around 20–40% of the maximum; for A19$_{47-55}$, epitopes levels did not peak until the end of the time course, following an almost identical profile to A19 protein expression. Of note the B8$_{20-27}$ epitope appeared to display a lag between peak of protein expression and peak of epitope presentation.
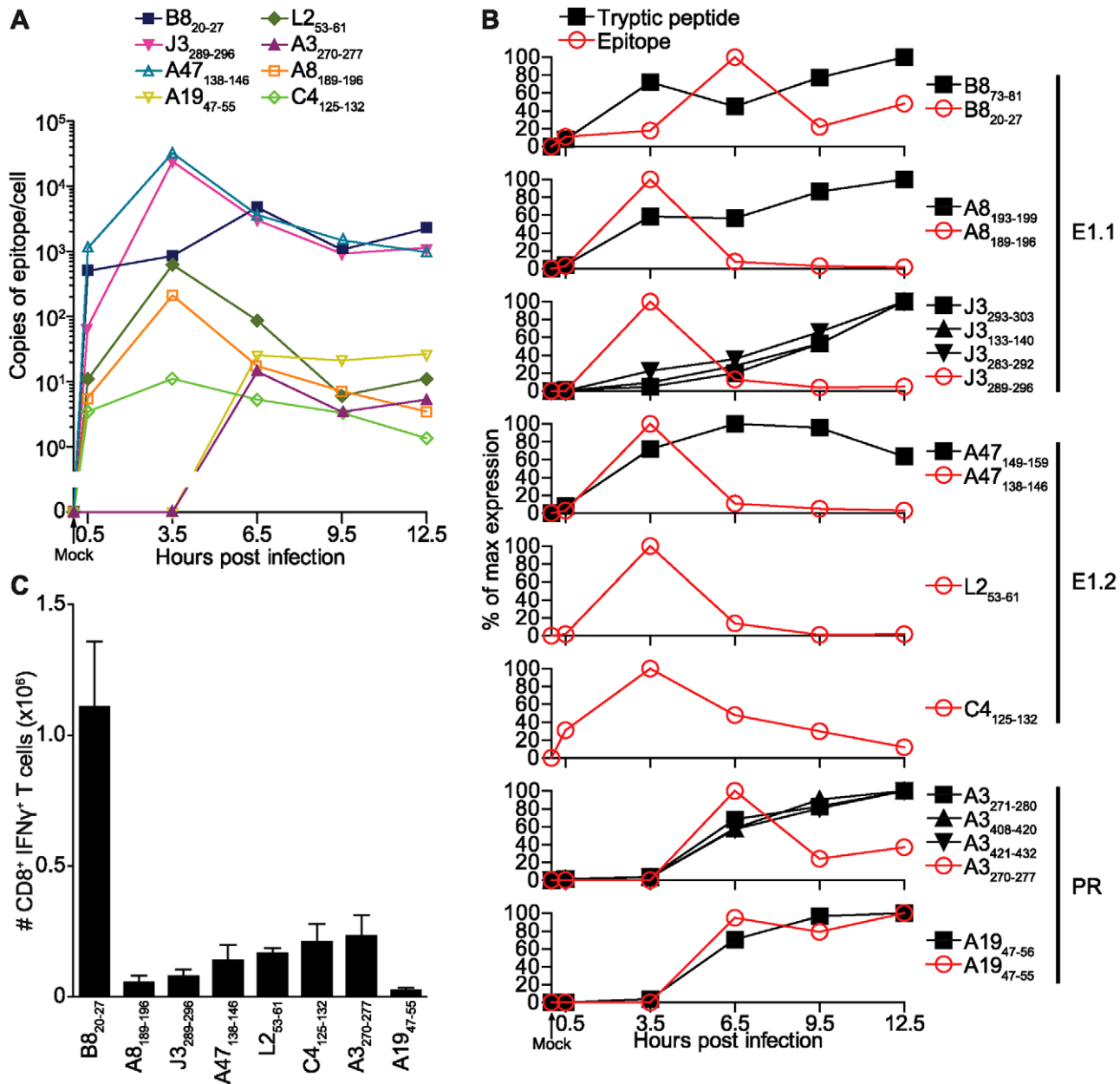
Figure 4. Kinetics of VACV antigen presentation. A) 1×10^8 DC2.4 cells/time point were infected with 5 pfu of VACV strain WR (or mock treated as time 0) and incubated for 0.5, 3.5, 6.5, 9.5 or 12.5 hours. MHC-peptide complexes were eluted at each time and epitope levels monitored by LC-MRM. Data show the copies of each epitope per cell. B) Epitope data from (A) expressed as the percentage of maximum levels alongside the relative kinetics of each source protein. C) $CD8^+$ T cell immunodominance hierarchy of WR infection 7 days after infection as determined brief stimulation with the peptides shown and ICS for IFNγ. Data are the mean and SEM of 3 mice and are representative of multiple experiments.
doi:10.1371/journal.ppat.1003129.g004

Next, *in vitro* protein and epitope presentation kinetics were correlated with $CD8^+$ T cell immunodominance *in vivo*. C57BL/6 mice were infected with VACV WR by the intraperitoneal route (i.p.) and 7 days after infection, the percentage of $CD8^+$ T cells responding to *ex vivo* stimulation with each peptide was determined by intracellular staining for IFNγ (Figure 4C). This method of epitope detection has recently been shown to have a linear range that covers responses to all the epitopes investigated here [44]. As previously reported [4,5], $B8_{20-27}$ dominated the response, $A19_{47-55}$ was the weakest and the remaining 6 epitopes formed an intermediate hierarchy. Here, where the onset, peak level

and longevity of epitope display were revealed (as opposed to the single time point for the WR-NP-S-GFP in Figure 3), there was still no obvious correlation between presentation and the $CD8^+$ T cell dominance hierarchy. Although the immunodominant $B8_{20-27}$ was one of the most robust epitopes in peak and persistence of presentation, it is similar in this respect to the subdominant $A47_{138-146}$ and $J3_{289-296}$. Further, $A3_{270-227}$ and $A8_{189-196}$, which are the next 2 peptides in the dominance hierarchy after $B8_{20-27}$, have very different presentation profiles with the former only appearing later (6.5 hpi) and having better persistence but a substantially lower (approximately 10-fold) peak than the latter.

Discussion

The use of liquid chromatography and mass spectrometry to detect MHC epitopes has a long heritage [e.g. [45–50]] yet it is only in recent years that techniques and instrumentation are beginning to surpass sensitivity and feasibility blockades to gain qualitative and quantitative insights into the immunopeptidome [24,32,51–53]. Use of LC-MRM methods to detect epitope presentation offers a large increase in sensitivity, but thus far has few precedents in the literature. LC-MRM analysis has rarely been used to examine antigen presentation with only a few examples examining melanoma epitopes [54] and measles virus epitopes [55]. We have recently further developed the methodology studying SIINFEKL presentation as a model antigen [32]. The current study is the first to comprehensively apply LC-MRM to study epitope presentation during virus infection, an inherently dynamic process. It is also the first to combine epitope and source antigen quantification from the same samples using LC-MRM. Our data provide extensions to and have implication for several aspects of antigen processing and anti-viral immunity and include:

1. Confirmation of epitopes mapped by prediction and synthetic peptides

The variable quality of epitope mapping data is a problem that is too frequently ignored [56,57]. Of the 8 epitopes examined here, 3 have been verified to the level of the source antigen and by peptide titration [4]. For the remaining 5, the only data available are from prediction and testing of peptides *in vitro* at relatively high concentration [5]. The nature of the MRM method leaves no ambiguity as to the sequence of peptides that are detected on infected cells and all 8 peptides have now been confirmed as the actual epitope presented on the surface of infected cells. Our data supports the value of the predictions and methods used to map such epitopes using overlapping synthetic peptides; but a wider comparison of the many epitopes published from a variety of viruses and other pathogens remain an important future goal.

2. Complexity of epitope kinetics

We show here that the abundance of virus epitopes varies massively from as low as 10 copies per cell to as high as >30,000 copies per cell. This variation is striking given that these are all relatively immunogenic peptides and responses to 6 of 8 epitopes fall within a two-fold range when measured using *ex vivo* assays (Figures 3C and 4C). The kinetics of epitope presentation was much more complex than that observed for single epitopes; not all epitopes were presented by 3.5 hours but all were there at 6.5 hpi consistent with data produced with mono-specific T cell lines [35]. Moreover, the dominant $B8_{20–27}$ epitope peaked at the 6.5 h time point, consistent with the rise in antigenicity seen on the infected cells between 5 and 7 hours (Figure 1B). To provide another view of epitope presentation, we have expressed our data in terms of the fraction of surface $H-2K^b$ occupied by the epitopes studied (Figure 5). To do this we have assumed a basal copy number for this MHC allomorph of 10^5 class I copies per cell, which although is likely to be conservative, is in line with published estimates [48,58]. Moreover, we have taken into account variation in cell surface MHC levels during the infection time course based on data collected under identical experimental conditions (Figure S5). This analysis highlights several striking features: First, as early as 3.5 hpi a very large proportion of all $H-2K^b$ on the infected cells are displaying virus-derived epitopes, which represents a very rapid and substantial change from the pre-infection immunopeptidome. This also contrasts with HIV infection, where the most noteworthy change after infection was the presentation of novel host epitopes

[16], suggesting that different viruses will have different impacts upon the immunopeptidome and thus may explain the very different evolution of immune responses to some viruses. Second, antigen presentation can be dominated by relatively few epitopes. At 3.5 hours after infection, presentation of just 2 virus epitopes ($A47_{138–146}$ and $J3_{289–296}$) can account for an estimated half of all $H-2K^b$ molecules. This domination of presentation by few virus epitopes has precedents, but has not been demonstrated so soon after infection [17]. Third, presentation is very dynamic, exemplified by the rise and fall of $A47_{138–146}$ and $J3_{289–296}$ from 0.5 to 6.5 hours. The rapid loss of presentation of these epitopes is intriguing because they both have relatively high affinity for $H-2K^b$ molecules (Table 1: IC_{50} of 0.61 and 1.2, respectively [59] (although our own data suggests $J3_{289–296}$ stabilises K^b poorly) and in each case the source protein continues to accumulate over this time. The loss of these peptides is not easy to reconcile with half life predictions for $H-2K^b$ ranging from a lower limit of around 48 minutes for empty forms [60], to estimates with peptides of moderate to high affinity of over 100 minutes [61]. However, half life is determined by the balance of association and dissociation rates [62], which are not fully known for these peptides. In our own studies (Figure S6), we find that a peptide's capacity for increased MHC stabilisation correlates roughly with the half life of that complex on the cell surface, yet neither of these factors can predict the kinetics observed in our study. This is perhaps not surprising given that such measured half lives are for cells in a steady state condition and not undergoing virus infection. As a virus such as VACV takes over all aspects of cell biology the supply of peptides will change abruptly. Just as virus epitopes rapidly replace those from the host, swamping the presentation capacity of cells at 3.5 hours, it is reasonable to suggest that the cascade of gene expression during infection is mirrored by successive waves of virus epitopes being presented. A final feature of Figure 5 is the comparison of data from cells infected with WR and WR-NP-S-GFP at the 6.5 hour time point. This shows very similar amounts of the native virus epitopes for both viruses, strongly supporting the validity of our normalization methodology. Whilst it also shows that SIINFEKL is more prevalent than any of the VACV epitopes in our study at 6.5 hours, compared with the $H-2K^b$ occupancy levels achieved by $A47_{138–146}$ and $J3_{289–296}$ at 3.5 hours it is by no means exceptional. Moreover, like $A47_{138–146}$ and $J3_{289–296}$, SIINFEKL is not as immunogenic as the $B8_{20–27}$ epitope.

3. Relationship between antigen and epitope levels

Previous studies have used various strategies to relate antigen expression or steady state levels to explain epitope abundance. On balance, studies comparing transcription and epitope levels show that the correlation between transcript levels and epitopes presented is not especially good [24,28]. Likewise, a proteomic approach using stable isotope labelling with amino acids in tissue culture (SILAC), found a limited correlation between the proteome and immunopeptidome [63]. A dynamic setting in which antigen levels are changing can provide more insight into the relationship between antigen and epitope levels. An example of this approach found that novel host cell epitopes appearing on HIV-infected cells was most likely related to the degradation of these proteins during infection and not level of expression [16]. In contrast, here we focus on virus antigens and epitopes and are able to correlate protein levels from the initiation of their synthesis. What is most clear from our study is that onset of epitope presentation is essentially coincident with neosynthesis of the source proteins. For 4 of the 6 epitopes where protein data were obtained, epitope abundance peaks before antigen abundance; for A19, epitope and protein kinetics were essentially coincident, and
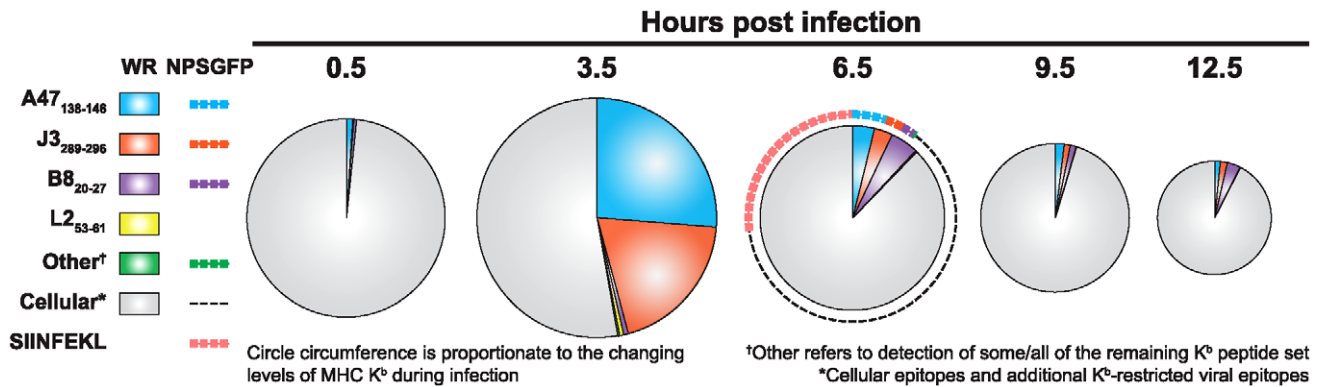
Figure 5. Cartoon depiction of the changes in vaccinia viral epitope presentation during infection. Circles represent infected cells at the indicated times post infection. Size is proportionate to the changing levels of MHC K^b during infection, relative to mock-infected cells.
doi:10.1371/journal.ppat.1003129.g005

for the remaining epitope ($B8_{20-27}$) protein abundance was found to peak first. Further, as noted above epitope turnover after the peak is often rapid, in contrast to the source proteins that typically continue to slowly rise or plateau. These data also demonstrate the power of the time course approach in that without the full kinetics of epitope and antigen levels, the conclusions would depend entirely on the time point chosen for analysis. The inescapable conclusion from our data is that epitope presentation is not well correlated with antigen abundance, but this is in part because of the rapid proteome dynamics in virus infected cells. The caveat here is that in our analysis we were not able to determine absolute protein abundance and so we cannot draw conclusions across the epitopes.

4. The source of virus epitopes

For many model antigens neo-synthesis of proteins and not their eventual degradation correlates with epitope production [25–27,64]. The rapid onset of epitope presentation that coincides with antigen expression in our study, strongly support this idea. Importantly we show this close coupling of expression and presentation for each of the 6 epitopes and these are derived from native virus proteins expressed in the normal course of infection. This means first, that the linkage of expression and presentation is indeed a general phenomenon. Second, that any concerns about previous findings being linked to the artificial nature of the model antigens or systems being used can now be discarded. What remains is to clearly reveal the identity of the source proteins: what fraction of these are the defective products predicted by the DRiP hypothesis versus other forms of rapidly degraded proteins, perhaps produced by the pioneer round of mRNA translation [65,66]. Either way, the efficiency implied by the appearance of 6 of our 8 epitopes as early as 30 minutes after infection suggests an exceptionally tight relationship between a subset of newly synthesised proteins and the antigen processing machinery. On the other hand, the presentation of post-translationally modified antigens in other studies presumably reflects that degradation of more mature protein species does contribute to the epitopes presented [67,68]. A full understanding of the fraction of epitopes derived from newly synthesized versus mature proteins awaits a full immunopeptidome-wide analysis. The behaviour of $B8_{20-27}$ is of interest in this respect: while onset of protein production and presentation were co-incident, peak presentation was delayed. We speculate that this antigen is processed by two pathways, with epitope being

produced both from nascent protein, but also from a pool of mature protein. So while we show here the benefits of broad-scale approaches in allowing the common themes to emerge, clearly much remains to be learnt from detailed analyses of individual antigens.

5. Antigenicity on infected cells and immunogenicity

In our experiments with both VACV viruses there is no correlation between levels of epitope display on infected cells and immunogenicity. Others have shown that epitope levels measured at a single time are not helpful in predicting the immunodominance hierarchy beyond suggesting that very low epitope levels can limit immunogenicity [47,69]. However, rate of epitope accumulation [69] and epitope off rates [70] or direct measurements of persistence [71] have all been suggested to be important determinants of immunogenicity. For the first time we are able to determine onset, peak and persistence of presentation for multiple epitopes and show that none of these parameters were useful indicators of immunogenicity. There are two main areas of explanation here. First we are using a cultured cell type that may or may not resemble the real APC for priming anti-VACV $CD8^+$ T cells. The balance of more recent studies suggests that during VACV infection most $CD8^+$ T cells are directly primed by infected DCs [29–31], but it remains possible that some epitopes may utilize cross priming [72]. If indeed cross priming is important, levels of epitope on cross priming DCs would almost certainly be different than those on infected cells and this might explain the discrepancy between our data on presentation and immunogenicity. Even if direct priming is the main pathway, numerous possible complications in presentation might be in play. More than one APC type might be involved and these might present varying levels of individual epitopes through an array of mechanisms. For example, differential immunoproteasome expression [73,74] or susceptibility to viral immune evasion mechanisms [75]. Infection might be aborted in some APCs and depending on the time that this occurs, epitopes from later classes of genes would not be presented. Of interest in this regard is that of the nearly 50 H-2^b-restricted epitopes mapped, only two very weak ones (far weaker than A19L examined here) are from genes with late promoters [5,43]. Further, epitope display on non-professional APCs might contribute to expansion of some specificities after priming [76]. It will be important to repeat our studies by harvesting APC directly *ex vivo* which will take into account epitopes acquired by any mechanism. Second, immunodominance

is a complicated business and is driven by factors other than availability of antigen. Precursor frequency for responding CD8^{+} T cells will always be a critical part of the explanation [77,78]. However, studies of VACV and influenza virus suggest that even epitope abundance and the T cell repertoire might not be enough to fully explain immunodominance [79,80]. Thus much work remains both on the antigen presentation and T cell sides of the immunodominance equation.

6. The value of individual epitopes as CD8^{+} T cell vaccine targets

The sharp peak of epitope presentation kinetics and delayed appearance of some epitopes are important factors to consider when using epitope abundance data to choose optimal vaccine targets. These considerations again highlight the importance of measuring presentation at multiple time points. Having said this, despite the vast difference in presentation levels, all the peptides in our study were shown to be highly protective (>70% survival) against a lethal VACV challenge when used as a sole immunogen [59]. As noted above, better studies to relate the protective capacity of epitopes with their display on infected cells will be subject to identifying and studying the relevant cell type *in vivo*.

In summary, the advances we present here in quantifying virus epitope abundance set a new benchmark in our understanding of antigen presentation during virus infection. The surprisingly dynamic nature of epitope display is a feature that has not been reported previously and has ramifications both for immunogenicity and use of epitopes as targets. This study is an important step toward the ultimate goal of quantifying epitope presentation *in vivo* which in turn is a requisite for a full understanding of anti-viral T cell responses and how they may be manipulated in future vaccines and other immunotherapies. Finally, the capacity to follow viral protein expression, induced host cell protein expression and antigen presentation will provide new avenues of research into the virus-host interaction and the role of immunoevasins and innate immune mechanisms in viral clearance.

Materials and Methods

Cell lines

The murine bone marrow-derived DC line DC2.4 [81] was provided as a kind gift from Professor Kenneth Rock (University of Massachusetts Medical School). The murine hybridoma Y-3 [82] secretes an anti-H-2K[b] monoclonal antibody and RMA-S is a TAP-deficient cell line derived from C57BL/6 mice [83]. Cells were maintained in RPMI or DMEM (Life Technologies) supplemented with 10% fetal bovine serum (FBS), 2 mM glutamine with or without 50 IU/ml penicillin and 50 µg/ml streptomycin (R10 or D10). BHK-21 and BS-C-1 were maintained in D10.

Virus production

VACV strains Western Reserve (VACV WR, ATCC #VR1354) and WR-NP-S-GFP were grown and titrated in BHK-21 and BS-C-1 cells respectively under DMEM with 2% FBS and 2 mM glutamine (D2) using standard methods. VACV WR and WR-NP-S-GFP were gifts of Bernard Moss, Jon Yewdell and Jack Bennink (all at NIH, Bethesda).

Virus infection

For LC-MRM experiments DC2.4 were washed twice with DMEM with no additions (D0), then 1×10^8 cells were infected at 10 plaque forming units (pfu) per cell in 2 ml D0 in round-bottom tubes for 30 minutes at 37°C with shaking. After this time the cells

were transferred to 50 ml tubes and 40 ml of warm D2 was added. The tubes were then incubated for the required time at 37°C with slow rotation. Cells were counted at the end of each incubation to account for any loss due to the method and snap frozen. For detection of K[b]-SIINFEKL and for use as stimulators prior to ICS, $1–5\times10^6$ of washed DC2.4 were infected with 10 pfu/cell of WR or WR-NP-S-GFP in 0.2 ml of D0 for 60 minutes at 37°C with shaking. After this time 10 ml of warm D2 was added and the tubes were incubated for the required time at 37°C and then placed on ice before staining with mAb 25D1.16 or use in intracellular cytokine staining (ICS).

Peptide synthesis

Peptides (>80% purity) were purchased from Genscript Corp (Piscataway, NJ) or Mimotopes (Clayton, Vic, Australia) and master stocks made with 100% DMSO at 1 mg/ml or greater. Dilutions were made in D0. For mass spectrometry, purified and lyophilised peptides were reconstituted in 100% DMSO at 5 mM and diluted with buffer A (0.1% formic acid in water) to stocks of 2.5 µM.

Flow cytometric staining of K[b]-SIINFEKL levels

DC2.4 cells (1×10^6) infected with WR-NP-S-GFP were incubated with mAb 25D1.16 conjugated to Allophycocyanin (eBioscience) [8,12] for 30 minutes on ice. Cells were washed and analysed by flow cytometry (LSR II, BD Biosciences) and analysis done using Flowjo software (Tree Star).

Stimulation and intracellular cytokine staining (ICS)

Splenocytes (1×10^6) from mice infected 7 days previously with VACV WR or WR-NP-S-GFP were incubated with 1) peptides at 10^{-7} M or 2) 2×10^5 DC2.4 cells infected with VACV (see above) in the wells of a 96-well plate at 37°C and 5% CO_2. 10 µg/ml brefeldin A was added after 1 hour, and the incubation continued for another 3–4 h. Plates were spun, medium was removed, and cells were stained for surface CD8 (clone 53–67, BD Biosciences) on ice for 20 minutes. Cells were washed, fixed with 1% paraformaldehyde solution, washed and then stained for intracellular IFNγ (clone XMG1.2, BD Biosciences) in PBS with 0.5% saponin at 4°C. Cells were washed and analysed by flow cytometry (LSR II, BD Biosciences) and analysis done using Flowjo software (Tree Star). Background staining determined using uninfected cells (generally around 0.1%) was subtracted from the values presented from infected samples. The fidelity of this method for enumeration of CD8^{+} T cell responses to acute VACV infection is supported by a recent study [44].

Purification of MHC-peptide complexes

Frozen cell pellets of DC2.4 were lysed by gentle resuspension in a total of 5 mls of 0.5% IGEPAL (Sigma), 50 mM Tris pH 8, 150 mM NaCl and protease inhibitors (Complete Protease Inhibitor Cocktail Tablet; Roche Molecular Biochemicals) and incubated with rotation for 1 hour at 4°C. Lysates were cleared by centrifugation at 16,000×g in a benchtop microfuge and MHC-peptide complexes immunoaffinity purified using Y-3 (anti-K[b]) monoclonal antibody bound to protein A-Sepharose, as previously described [32,84]. Bound complexes were eluted by acidification with 10% acetic acid. The mixture of peptides and MHC protein chains was fractionated on a 4.6 mm internal diameter×50 mm long reversed-phase C18 HPLC column (Chromolith Speed Rod, Merck) using an ÄKTAmicro HPLC system (GE Healthcare) running on a mobile phase buffer A of 0.1% trifluoroacetic acid (TFA) and buffer B of 80% acetonitrile/0.1% TFA and at a flow

rate of 1 ml/min with peptides separated across a gradient of 2% B to 45% B over the course of 20 minutes, collecting 500 µl fractions.

FASP protein purification and tryptic digestion

Lysate flow-through following immunoaffinity purification was used to detect cellular and VACV proteins. 200 µl of flow-through was treated with the reducing agent (tris(2-carboxyethyl)phosphine (TCEP) at a final concentration of 5 mM and sample heated to 60°C for 30 minutes. 30 µl of sample was then loaded onto a FASP protein digestion kit column (Protein Discovery) [33] and tryptic digestion of proteins carried out as per the manufacturer's instructions. Digested proteins were eluted from the column with 50 µl of 0.5 M sodium chloride into 80 µl of 50 mM ammonium bicarbonate. 10-fold dilutions of the eluate (starting from 10 µl neat, to a 1/1000 dilution) were made to a 20 µl volume with mass spectrometry buffer A (0.1% TFA in water) and analysed by LC-MRM as described below (see *Liquid chromatography mass spectrometry*).

Design of VACV MRMs

MRM transitions for 8 VACV epitopes, restricted through murine K^b MHC class I molecules, were designed through spiking 200 fmol of synthetic versions of each peptide into an AB-SCIEX QTRAP 5500 mass spectrometer (Table S1 and Figure S1). Each peptide was initially analysed in EMS scanning mode to determine the predominant precursor (Q1) ion. Peptides were then analysed in EPI scanning mode across a range of collision energies (CEs) to determine the optimal CE resulting in the highest intensity fragment ions in Q3. At least four Q3 ions were chosen per peptide to eliminate isobaric peptides triggering false-positive MRMs, and each Q3 ion was fine-tuned for optimal intensity using the method of Sherwood et al [85]. All MRMs were built into a single method which also included the previously described MRMs for SIINFEKL and isotopically-labelled (AQUA) SIIN*FEKL [32].

Design of theoretical MRMs for VACV and murine protein antigen detection

Skyline [39] v1.2.0.3245 was used to build an initial library of MRMs targeting proteotypic tryptic fragments for each VACV protein from which epitopes in this study were derived (Table S2 and Figure S4). Up to 3 tryptic fragments were selected per protein, with at least 3 transitions per peptide. MRMs for each peptide were further refined upon their detection. 12 tryptic murine peptides (corresponding to 8 proteins) were used to normalise protein levels across the timecourse (Table S3 and Figure S3).

Liquid chromatography mass spectrometry

Following peptide elution, samples were concentrated using a Labconco Centrivac concentrator, set to 40°C. Samples were concentrated down to a volume of <10 µl and then all equalised to 20 µl through the addition of 0.1% formic acid in water (buffer A), sonicated in a water bath for 10 minutes and centrifuged for 10 minutes at 13,000 rpm prior to samples being stored in mass spectrometry vials at 4°C for immediate analysis by mass spectrometry. An AB SCIEX QTRAP 5500 mass spectrometer was used for MRM detection, coupled on-line to a Tempo nano LC (Eksigent) autosampler and cHiPLC nanoflex (Eksigent). 20 µl samples were injected and loaded onto a trap column (200 µm×0.5 mm ChromXP C18-CL 3 µm 120 Å; Eksigent part number 804-00006) at a flow rate of 10 µl/min in 98% buffer A

for 10 minutes. For on-line fractionation of samples onto the mass spectrometer, samples were eluted from the trap column and over a cHiPLC column (75 µm×15 cm ChromXP C18-CL 3 µm 120 Å; Eksigent part number 804-00001) at 300 nl/min under the following buffer B (95% acetonitrile, 0.1% formic acid in water) gradient conditions: 0–3 min 2–10% B, 3–33 min 10–40% B, 33–36 min 40–80% B, 36–38 min hold at 80% B, 38–39 min 80–2% B, followed by equilibration at 2% B until the end of the run at 48 min. The QTRAP 5500 was operated in MRM mode in unit resolution for Q1 and Q3, coupled to an information-dependent acquisition (IDA) criterion set to trigger an EPI scan (10,000 Da/sec; rolling CE; unit resolution) following any MRM transition exceeding 500 counts (ignoring the triggering MRM transition for 3 seconds thereafter).

Mass spectrometry data analysis

Data analysis was performed using a combination of Analyst v1.5.2, Peakview v1.1 and Multiquant v2.0.2 (AB SCIEX).

RMA-S stabilisation assay

RMA-S cells were used to measure the capacity for each epitope to stabilise MHC K^b cells, as described previously [86]. Briefly, cells were grown overnight at 26°C to allow expression of peptide receptive class I molecules on the surface of cells. The following morning, decreasing concentrations of peptide were exogenously loaded onto the cells for 1 hour and then the cells transferred to 37°C for 2 hours to allow unloaded H-2K^b molecules to dissociate. Cells were then stained with the K^b-specific monoclonal antibody Y-3, followed by secondary detection with a FITC-conjugated anti-murine IgG antibody (Merck Millipore; AQ326-K) and visualisation by flow cytometry. For measuring the time course of epitope stabilisation, cells were grown and labelled as above with 1 µM of peptide for 1 hour at 26°C, washed, and then incubated for the indicated amount of time. Class I molecules were detected as in the standard stabilisation assay. Data was analysed using FlowJo software (TreeStar).

MHC expression analysis during virus infection

DC2.4 cells (2×10^7) were infected with VACV-WR at an m.o.i. of 5 in 500 µl of serum-free DMEM for 30 minutes. Infected cells were then transferred to 40 ml DMEM supplemented with 2% FCS. The tubes were then incubated for the required time at 37°C with slow rotation. Cells were centrifuged, incubated with Fc block (BD Biosciences; clone 2.4G2) for 20 minutes at 4°C. Cells were washed once and stained with PE-conjugated anti-H2-Kb (Biolegend; AF6-88.5) for 30 minutes at 4°C. Cells were wash and fixed with paraformaldehyde at room temperature for 20 minutes. Cells were washed and analysed by flow cytometry (LSR II, BD Biosciences) and analysed using FlowJo software (Tree Star).

Ethics

All experiments were done according to Australian NHMRC guidelines contained within the Australian Code of Practice for the Care and Use of Animals for Scientific Purposes and under approvals F-BMB-38.8 and A2011-01 from the Australian National University Animal Ethics and Experimentation Committee.

Supporting Information

Figure S1 MS and MS/MS analysis of synthetic VACV peptides for MRM design. 200 fmol of each VACV peptide was analysed individually by a QTRAP 5500 operating in

enhanced MS (EMS) mode in order to determine the dominant precursor ion (upper panel for each peptide; precursor ion charge is indicated). Subsequently, a full enhanced product ion (EPI) scan (80–1000 m/z range) across a range of collision energy (CE) values was triggered following detection of the dominant precursor (lower panel for each peptide; a single CE is shown for clarity, although different CEs were used for optimal product generation – refer to Table S1). Further refinement of optimal MRM conditions was achieved using a method adapted from Sherwood *et al.* (*Sherwood et al., 2009*). At least 4 Q3 product ions (purple lines) were chosen per peptide in order to practically eliminate false-positive signal due to the presence of isobaric peptide species in MHC eluates.
(TIF)

Figure S2 Eluting RP-HPLC fractions for each epitope. 1 nmol of each peptide was spiked individually onto a 4.6 mm internal diameter×50 mm long reversed-phase C18 HPLC column (Chromolith Speed Rod, Merck) using an ÄKTAmicro HPLC system (GE Healthcare) running on a mobile phase buffer A of 0.1% trifluoroacetic acid (TFA) and buffer B of 80% acetonitrile/0.1% TFA and at a flow rate of 1 ml/min. These conditions are identical to those used in the separation of peptides following MHC elution and therefore determines the RP-HPLC fraction (indicated above each chromatographic peak) which contains each VACV epitope. Peptides were read at an absorbance of 215 nm.
(TIF)

Figure S3 The use of murine protein MRMs for the protein normalisation during VACV infection. In order to accurately measure relative levels of VACV protein expression during infection (see Supporting Information Figure S4) it was necessary to concurrently measure host cellular protein levels as references for normalisation. Following protein lysate reduction and alkylation with iodoacetamide, levels of twelve tryptic peptides (corresponding to 8 murine proteins) were measured using the MRM transitions described in Table S2. A) Multiplexed detection of each murine tryptic peptide. Example data is from mock infection and a single MRM transition is shown for each peptide for clarity. * indicates false-positive signal peaks. Protein name and peptide sequence (in parentheses) are indicated for each peak. B) Detection levels (calculated from sum MRM area per peptide) of each murine peptide during the infection timecourse relative to the level observed from mock infection. C) Murine tryptic peptide data plotted as individual points showing mean +/− SEM. Cell count (plotted relative to mock on the same scale) is overlaid. D) Normalisation factor (mock set to 1) for each step of the time course calculated by taking the inverse of the detection level relative to mock from (C). Data shows mean +/− SEM, where the mean was used as the normalisation value for calculating VACV protein abundance. The full protein descriptors are defined in Table S2.
(TIF)

Figure S4 Kinetics of VACV protein expression during infection. VACV proteins were detected using the MRM transitions described in Table S3. A) Raw (non-normalised) MRM detection intensities at each stage of infection. MRM trace y-axes are set to the maximum detected value for each protein. B) Raw and normalised (see Supporting Information Figure S3) VACV protein levels, plotted as a percentage of maximum.
(TIF)

Figure S5 Surface MHC class I K^b levels during VACV WR infection. DC2.4 cells were infected with VACV strain WR and incubated for the indicated times at which point cell surface MHC class I K^b molecules were visualised by flow cytometry. Data is plotted as the percentage expression relative to mock-infected cells at time 0. Values are mean of triplicate samples +/− SEM and are representative of one of two independent experiments.
(TIF)

Figure S6 Epitope stabilisation assay of VACV peptides. A) RMA-S cells were grown overnight at 26°C to induce maximal empty class I expression and then exogenously labelled with the indicated titrated concentrations of each synthetic VACV peptide for 1 hour and then transferred to 37°C for 2 hours. Stabilised cell surface MHC class I complexes were visualised by flow cytometry. B) Epitope stabilisation across 6.5 hours was carried out following labelling of stabilised empty class I molecules with 1 μM of synthetic peptide, washing cells and incubating at 37°C for the indicated times. Stabilised cell surface MHC class I complexes were visualised by flow cytometry. Estimated half-lives for each peptide-MHC complex are as follows: $B8_{20-27}$, 5 hrs; $J3_{289-296}$, 5 hrs; $A47_{138-146}$, 5.5 hrs; $A19_{47-55}$, 7 hrs; $L2_{53-61}$, 12 hrs; $A3_{270-277}$, 5 hrs; $A8_{189-196}$, 5 hrs; $C4_{125-132}$, 4.5 hrs. All data are mean of triplicate values +/− SEM and are representative of at least two independent experiments.
(TIF)

Table S1 MRM transitions used to monitor for VACV epitopes. Target epitope position with each protein is indicated, along with epitope amino acid sequence, Q1 and Q3 m/z, the dwell time that the QTRAP instruments spends on each transition and the optimal collision energy (CE) for each transition.
(DOCX)

Table S2 MRM transitions used to monitor for murine tryptic peptides. Target protein and peptide amino acid sequence is indicated, along with the Q1 and Q3 m/z, the dwell time that the QTRAP instruments spends on each transition and the optimal collision energy (CE) for each transition.
(DOCX)

Table S3 MRM transitions used to monitor for VACV tryptic peptides. Target protein and peptide amino acid sequence is indicated, along with the Q1 and Q3 m/z, the dwell time that the QTRAP instruments spends on each transition and the optimal collision energy (CE) for each transition.
(DOCX)

Author Contributions

Conceived and designed the experiments: NPC DCT AWP. Performed the experiments: NPC SAS YCW LCWL IEAF CTT NLD. Analyzed the data: NPC DCT AWP. Wrote the paper: NPC DCT AWP.

References

1. Purcell AW, Elliott T (2008) Molecular machinations of the MHC-I peptide loading complex. Curr Opin Immunol 20: 75–81.
2. Dudek NL, Perlmutter P, Aguilar MI, Croft NP, Purcell AW (2010) Epitope discovery and their use in peptide based vaccines. Curr Pharm Des 16: 3149–3157.
3. Yewdell JW (2006) Confronting complexity: real-world immunodominance in antiviral CD8+ T cell responses. Immunity 25: 533–543.
4. Tscharke DC, Karupiah G, Zhou J, Palmore T, Irvine KR, et al. (2005) Identification of poxvirus CD8+ T cell determinants to enable rational design and characterization of smallpox vaccines. J Exp Med 201: 95–104.
5. Moutaftsi M, Peters B, Pasquetto V, Tscharke DC, Sidney J, et al. (2006) A consensus epitope prediction approach identifies the breadth of murine T(CD8+)-cell responses to vaccinia virus. Nat Biotechnol 24: 817–819.

6. Vyas JM, Van der Veen AG, Ploegh HL (2008) The known unknowns of antigen processing and presentation. Nat Rev Immunol 8: 607–618.

7. Purcell AW, McCluskey J, Rossjohn J (2007) More than one reason to rethink the use of peptides in vaccine design. Nat Rev Drug Discov 6: 404–414.

8. Princiotta MF, Finzi D, Qian SB, Gibbs J, Schuchmann S, et al. (2003) Quantitating protein synthesis, degradation, and endogenous antigen processing. Immunity 18: 343–354.

9. Anton LC, Yewdell JW, Bennink JR (1997) MHC class I-associated peptides produced from endogenous gene products with vastly different efficiencies. J Immunol 158: 2535–2542.

10. Dolan BP, Sharma AA, Gibbs JS, Cunningham TJ, Bennink JR, et al. (2012) MHC class I antigen processing distinguishes endogenous antigens based on their translation from cellular vs. viral mRNA. Proceedings of the National Academy of Sciences 109: 7025–7030.

11. Pang KC, Wei JQZ, Chen W (2006) Dynamic quantification of MHC class I–peptide presentation to CD8+ T cells via intracellular cytokine staining. Journal of Immunological Methods 311: 12–18.

12. Porgador A, Yewdell JW, Deng Y, Bennink JR, Germain RN (1997) Localization, quantitation, and in situ detection of specific peptide-MHC class I complexes using a monoclonal antibody. Immunity 6: 715–726.

13. Lev A, Princiotta MF, Zanker D, Takeda K, Gibbs JS, et al. (2010) Compartmentalized MHC class I antigen processing enhances immunosurveillance by circumventing the law of mass action. Proc Natl Acad Sci U S A 107: 6964–6969.

14. Makler O, Oved K, Netzer N, Wolf D, Reiter Y (2010) Direct visualization of the dynamics of antigen presentation in human cells infected with cytomegalovirus revealed by antibodies mimicking TCR specificity. Eur J Immunol 40: 1552–1565.

15. Michaeli Y, Denkberg G, Sinik K, Lantzy L, Chih-Sheng C, et al. (2009) Expression hierarchy of T cell epitopes from melanoma differentiation antigens: unexpected high level presentation of tyrosinase-HLA-A2 Complexes revealed by peptide-specific, MHC-restricted, TCR-like antibodies. J Immunol 182: 6328–6341.

16. Hickman HD, Luis AD, Bardet W, Buchli R, Battson CL, et al. (2003) Cutting edge: class I presentation of host peptides following HIV infection. J Immunol 171: 22–26.

17. van Els CA, Herberts CA, van der Heeft E, Poelen MC, van Gaans-van den Brink JA, et al. (2000) A single naturally processed measles virus peptide fully dominates the HLA-A*0201-associated peptide display and is mutated at its anchor position in persistent viral strains. Eur J Immunol 30: 1172–1181.

18. Tellam J, Smith C, Rist M, Webb N, Cooper L, et al. (2008) Regulation of protein translation through mRNA structure influences MHC class I loading and T cell recognition. Proc Natl Acad Sci U S A 105: 9319–9324.

19. Granados DP, Yahyaoui W, Laumont CM, Daouda T, Muratore-Schroeder TL, et al. (2012) MHC I-associated peptides preferentially derive from transcripts bearing miRNA response elements. Blood 119: e181–191.

20. de Verteuil D, Granados DP, Thibault P, Perreault C (2012) Origin and plasticity of MHC I-associated self peptides. Autoimmun Rev 11: 627–635.

21. Dolan BP, Bennink JR, Yewdell JW (2011) Translating DRiPs: progress in understanding viral and cellular sources of MHC class I peptide ligands. Cell Mol Life Sci 68: 1481–1489.

22. Dolan BP, Li L, Veltri CA, Ireland CM, Bennink JR, et al. (2011) Distinct pathways generate peptides from defective ribosomal products for CD8+ T cell immunosurveillance. J Immunol 186: 2065–2072.

23. Farfan-Arribas DJ, Stern LJ, Rock KL (2012) Using intein catalysis to probe the origin of major histocompatibility complex class I-presented peptides. Proc Natl Acad Sci U S A 109: 16998–7003.

24. Fortier MH, Caron E, Hardy MP, Voisin G, Lemieux S, et al. (2008) The MHC class I peptide repertoire is molded by the transcriptome. J Exp Med 205: 595–610.

25. Reits EA, Vos JC, Gromme M, Neefjes J (2000) The major substrates for TAP in vivo are derived from newly synthesized proteins. Nature 404: 774–778.

26. Schubert U, Anton LC, Gibbs J, Norbury CC, Yewdell JW, et al. (2000) Rapid degradation of a large fraction of newly synthesized proteins by proteasomes. Nature 404: 770–774.

27. Khan S, de Giuli R, Schmidtke G, Bruns M, Buchmeier M, et al. (2001) Cutting edge: neosynthesis is required for the presentation of a T cell epitope from a long-lived viral protein. J Immunol 167: 4801–4804.

28. Weinzierl AO, Lemmel C, Schoor O, Muller M, Kruger T, et al. (2007) Distorted relation between mRNA copy number and corresponding major histocompatibility complex ligand density on the cell surface. Mol Cell Proteomics 6: 102–113.

29. Norbury CC, Malide D, Gibbs JS, Bennink JR, Yewdell JW (2002) Visualizing priming of virus-specific CD8+ T cells by infected dendritic cells in vivo. Nat Immunol 3: 265–271. Epub 2002 Feb 2004.

30. Hickman HD, Takeda K, Skon CN, Murray FR, Hensley SE, et al. (2008) Direct priming of antiviral CD8+ T cells in the peripheral interfollicular region of lymph nodes. Nat Immunol 9: 155–165. Epub 2008 Jan 2013.

31. Xu RH, Remakus S, Ma X, Roscoe F, Sigal LJ (2010) Direct presentation is sufficient for an efficient anti-viral CD8+ T cell response. PLoS Pathog 6: e1000768.

32. Tan CT, Croft NP, Dudek NL, Williamson NA, Purcell AW (2011) Direct quantitation of MHC-bound peptide epitopes by selected reaction monitoring. Proteomics 11: 2336–2340.

33. Wisniewski JR, Zougman A, Nagaraj N, Mann M (2009) Universal sample preparation method for proteome analysis. Nat Methods 6: 359–362.

34. Norbury CC, Basta S, Donohue KB, Tscharke DC, Princiotta MF, et al. (2004) CD8+ T cell cross-priming via transfer of proteasome substrates. Science 304: 1318–1321.

35. Kastenmuller W, Gasteiger G, Gronau JH, Baier R, Ljapoci R, et al. (2007) Cross-competition of CD8+ T cells shapes the immunodominance hierarchy during boost vaccination. J Exp Med 204: 2187–2198. Epub 2007 Aug 2120.

36. Lange V, Picotti P, Domon B, Aebersold R (2008) Selected reaction monitoring for quantitative proteomics: a tutorial. Mol Syst Biol 4: 222.

37. Dudek NL, Tan CT, Gorasia DG, Croft NP, Illing PT, et al. (2012) Constitutive and Inflammatory Immunopeptidome of Pancreatic beta-Cells. Diabetes 61: 3018–25.

38. Unwin RD, Griffiths JR, Leverentz MK, Grallert A, Hagan IM, et al. (2005) Multiple reaction monitoring to identify sites of protein phosphorylation with high sensitivity. Mol Cell Proteomics 4: 1134–1144.

39. MacLean B, Tomazela DM, Shulman N, Chambers M, Finney GL, et al. (2010) Skyline: an open source document editor for creating and analyzing targeted proteomics experiments. Bioinformatics 26: 966–968.

40. Schwanhausser B, Busse D, Li N, Dittmar G, Schuchhardt J, et al. (2010) Global quantification of mammalian gene expression control. Nature 473: 337–342.

41. Yang Z, Bruno DP, Martens CA, Porcella SF, Moss B (2010) Simultaneous high-resolution analysis of vaccinia virus and host cell transcriptomes by deep RNA sequencing. Proc Natl Acad Sci U S A 107: 11513–11518.

42. Assarsson E, Greenbaum JA, Sundstrom M, Schaffer L, Hammond JA, et al. (2008) Kinetic analysis of a complete poxvirus transcriptome reveals an immediate-early class of genes. Proc Natl Acad Sci U S A 105: 2140–2145.

43. Yang Z, Reynolds SE, Martens CA, Bruno DP, Porcella SF, et al. (2011) Expression profiling of the intermediate and late stages of poxvirus replication. J Virol 85: 9899–9908. Epub 2011 Jul 9827.

44. Flesch IE, Hollett NA, Wong YC, Tscharke DC (2012) Linear fidelity in quantification of anti-viral CD8+ T cells. PLoS One 7: e39533. Epub 32012 Jun 39520.

45. Chicz RM, Urban RG, Lane WS, Gorga JC, Stern LJ, et al. (1992) Predominant naturally processed peptides bound to HLA-DR1 are derived from MHC-related molecules and are heterogeneous in size. Nature 358: 764–768.

46. Cox AL, Skipper J, Chen Y, Henderson RA, Darrow TL, et al. (1994) Identification of a peptide recognized by five melanoma-specific human cytotoxic T cell lines. Science 264: 716–719.

47. Crotzer VL, Christian RE, Brooks JM, Shabanowitz J, Settlage RE, et al. (2000) Immunodominance among EBV-derived epitopes restricted by HLA-B27 does not correlate with epitope abundance in EBV-transformed B-lymphoblastoid cell lines. J Immunol 164: 6120–6129.

48. Hunt DF, Henderson RA, Shabanowitz J, Sakaguchi K, Michel H, et al. (1992) Characterization of peptides bound to the class I MHC molecule HLA-A2.1 by mass spectrometry. Science 255: 1261–1263.

49. Rudensky A, Preston-Hurlburt P, Hong SC, Barlow A, Janeway CA, Jr. (1991) Sequence analysis of peptides bound to MHC class II molecules. Nature 353: 622–627.

50. Urban RG, Chicz RM, Lane WS, Strominger JL, Rehm A, et al. (1994) A subset of HLA-B27 molecules contains peptides much longer than nonamers. Proc Natl Acad Sci U S A 91: 1534–1538.

51. Scull KE, Dudek NL, Corbett AJ, Ramarathinam SH, Gorasia DG, et al. (2012) Secreted HLA recapitulates the immunopeptidome and allows in-depth coverage of HLA A*02:01 ligands. Mol Immunol 51: 136–142.

52. Kincaid EZ, Che JW, York I, Escobar H, Reyes-Vargas E, et al. (2011) Mice completely lacking immunoproteasomes show major changes in antigen presentation. Nat Immunol 13: 129–135.

53. Caron E, Vincent K, Fortier MH, Laverdure JP, Bramoulle A, et al. (2011) The MHC I immunopeptidome conveys to the cell surface an integrative view of cellular regulation. Mol Syst Biol 7: 533.

54. Hogan KT, Sutton JN, Chu KU, Busby JA, Shabanowitz J, et al. (2005) Use of selected reaction monitoring mass spectrometry for the detection of specific MHC class I peptide antigens on A3 supertype family members. Cancer Immunol Immunother 54: 359–371.

55. Herberts CA, Meiring HM, van Gaans-van den Brink JA, van der Heeft E, Poelen MC, et al. (2003) Dynamics of measles virus protein expression are reflected in the MHC class I peptide display. Mol Immunol 39: 567–575.

56. Yewdell JW (2005) The seven dirty little secrets of major histocompatibility complex class I antigen processing. Immunol Rev 207: 8–18.

57. Yuen TJ, Flesch IE, Hollett NA, Dobson BM, Russell TA, et al. (2010) Analysis of A47, an immunoprevalent protein of vaccinia virus, leads to a reevaluation of the total antiviral CD8+ T cell response. J Virol 84: 10220–10229.

58. Neefjes J, Jongsma ML, Paul P, Bakke O (2011) Towards a systems understanding of MHC class I and MHC class II antigen presentation. Nat Rev Immunol 11: 823–836.

59. Moutaftsi M, Salek-Ardakani S, Croft M, Peters B, Sidney J, et al. (2009) Correlates of protection efficacy induced by vaccinia virus-specific CD8+ T-cell epitopes in the murine intranasal challenge model. Eur J Immunol 39: 717–722.

60. Ljunggren HG, Stam NJ, Ohlen C, Neefjes JJ, Hoglund P, et al. (1990) Empty MHC class I molecules come out in the cold. Nature 346: 476–480.

61. Howarth M, Williams A, Tolstrup AB, Elliott T (2004) Tapasin enhances MHC class I peptide presentation according to peptide half-life. Proc Natl Acad Sci U S A 101: 11737–11742.

62. Eisen HN, Hou XH, Shen C, Wang K, Tanguturi VK, et al. (2012) Promiscuous binding of extracellular peptides to cell surface class I MHC protein. Proc Natl Acad Sci U S A 109: 4580–4585.

63. Milner E, Barnea E, Beer I, Admon A (2006) The turnover kinetics of major histocompatibility complex peptides of human cancer cells. Mol Cell Proteomics 5: 357–365.

64. Yewdell JW, Anton LC, Bennink JR (1996) Defective ribosomal products (DRiPs): a major source of antigenic peptides for MHC class I molecules? J Immunol 157: 1823–1826.

65. Apcher S, Daskalogianni C, Lejeune F, Manoury B, Imhoos G, et al. (2011) Major source of antigenic peptides for the MHC class I pathway is produced during the pioneer round of mRNA translation. Proc Natl Acad Sci U S A 108: 11572–11577.

66. Yewdell JW (2011) DRiPs solidify: progress in understanding endogenous MHC class I antigen processing. Trends Immunol 32: 548–558.

67. Mannering SI, Harrison LC, Williamson NA, Morris JS, Thearle DJ, et al. (2005) The insulin A-chain epitope recognized by human T cells is posttranslationally modified. J Exp Med 202: 1191–1197.

68. Petersen J, Purcell AW, Rossjohn J (2009) Post-translationally modified T cell epitopes: immune recognition and immunotherapy. J Mol Med (Berl) 87: 1045–1051.

69. Chen W, Anton LC, Bennink JR, Yewdell JW (2000) Dissecting the multifactorial causes of immunodominance in class I-restricted T cell responses to viruses. Immunity 12: 83–93.

70. van der Burg SH, Visseren MJ, Brandt RM, Kast WM, Melief CJ (1996) Immunogenicity of peptides bound to MHC class I molecules depends on the MHC-peptide complex stability. J Immunol 156: 3308–3314.

71. Yoshimura Y, Yadav R, Christianson GJ, Ajayi WU, Roopenian DC, et al. (2004) Duration of alloantigen presentation and avidity of T cell antigen recognition correlate with immunodominance of CTL response to minor histocompatibility antigens. J Immunol 172: 6666–6674.

72. Basta S, Chen W, Bennink JR, Yewdell JW (2002) Inhibitory effects of cytomegalovirus proteins US2 and US11 point to contributions from direct priming and cross-priming in induction of vaccinia virus-specific CD8(+) T cells. J Immunol 168: 5403–5408.

73. Chen W, Norbury CC, Cho Y, Yewdell JW, Bennink JR (2001) Immunoproteasomes shape immunodominance hierarchies of antiviral CD8(+) T cells at the levels of T cell repertoire and presentation of viral antigens. J Exp Med 193: 1319–1326.

74. Groettrup M, Soza A, Eggers M, Kuehn L, Dick TP, et al. (1996) A role for the proteasome regulator PA28alpha in antigen presentation. Nature 381: 166–168.

75. Holtappels R, Podlech J, Pahl-Seibert MF, Julch M, Thomas D, et al. (2004) Cytomegalovirus misleads its host by priming of CD8 T cells specific for an epitope not presented in infected tissues. J Exp Med 199: 131–136.

76. Tatum AM, Watson AM, Schell TD (2010) Direct presentation regulates the magnitude of the CD8+ T cell response to cell-associated antigen through prolonged T cell proliferation. J Immunol 185: 2763–2772.

77. Obar JJ, Khanna KM, Lefrancois L (2008) Endogenous naive CD8+ T cell precursor frequency regulates primary and memory responses to infection. Immunity 28: 859–869.

78. Kotturi MF, Scott I, Wolfe T, Peters B, Sidney J, et al. (2008) Naive precursor frequencies and MHC binding rather than the degree of epitope diversity shape CD8+ T cell immunodominance. J Immunol 181: 2124–2133.

79. La Gruta NL, Rothwell WT, Cukalac T, Swan NG, Valkenburg SA, et al. (2010) Primary CTL response magnitude in mice is determined by the extent of naive T cell recruitment and subsequent clonal expansion. J Clin Invest 120: 1885–1894.

80. Flesch IE, Woo WP, Wang Y, Panchanathan V, Wong YC, et al. (2010) Altered CD8(+) T cell immunodominance after vaccinia virus infection and the naive repertoire in inbred and F(1) mice. J Immunol 184: 45–55.

81. Shen Z, Reznikoff G, Dranoff G, Rock KL (1997) Cloned dendritic cells can present exogenous antigens on both MHC class I and class II molecules. J Immunol 158: 2723–2730.

82. Hammerling GJ, Rusch E, Tada N, Kimura S, Hammerling U (1982) Localization of allodeterminants on H-2Kb antigens determined with monoclonal antibodies and H-2 mutant mice. Proc Natl Acad Sci U S A 79: 4737–4741.

83. Townsend A, Ohlen C, Foster L, Bastin J, Ljunggren HG, et al. (1989) A mutant cell in which association of class I heavy and light chains is induced by viral peptides. Cold Spring Harb Symp Quant Biol 54: 299–308.

84. Purcell AW, Gorman JJ, Garcia-Peydro M, Paradela A, Burrows SR, et al. (2001) Quantitative and qualitative influences of tapasin on the class I peptide repertoire. J Immunol 166: 1016–1027.

85. Sherwood CA, Eastham A, Lee LW, Risler J, Mirzaei H, et al. (2009) Rapid optimization of MRM-MS instrument parameters by subtle alteration of precursor and product m/z targets. J Proteome Res 8: 3746–3751.

86. Webb AI, Borg NA, Dunstone MA, Kjer-Nielsen L, Beddoe T, et al. (2004) The structure of H-2K(b) and K(bm8) complexed to a herpes simplex virus determinant: evidence for a conformational switch that governs T cell repertoire selection and viral resistance. J Immunol 173: 402–409.